Jae-Ha Lee
Mechanics of Materials and Design Laboratory,
Department of Materials Engineering,
Gangneung-Wonju National University,
Gangwon-do, Gangneung 25457, South Korea

Hyunho Shin[1]
Mechanics of Materials and Design Laboratory,
Department of Materials Engineering,
Gangneung-Wonju National University,
Gangwon-do, Gangneung 25457, South Korea
e-mail: hshin@gwnu.ac.kr

Jong-Bong Kim[1]
Computational Mechanics and
Design Laboratory,
Department of Mechanical and
Automotive Engineering,
Seoul National University of
Science and Technology,
Nowon-gu, Seoul 01811, South Korea
e-mail: jbkim@seoultech.ac.kr

Ju-Young Kim
Poongsan Defense R&D Institute,
Yuseong-gu, Daejeon 34027, South Korea

Sung-Taek Park
Poongsan Defense R&D Institute,
Yuseong-gu, Daejeon 34027, South Korea

Gwang-Lyeon Kim
Poongsan Defense R&D Institute,
Yuseong-gu, Daejeon 34027, South Korea

Kyeong-Won Oh
Defense Industry Technology Center,
Yongsan-gu, Seoul 04353, South Korea

Determination of the Flow Stress–Strain Curves of Aluminum Alloy and Tantalum Using the Compressive Load–Displacement Curves of a Hat-Type Specimen

The load–displacement curves of an aluminum alloy and tantalum were determined using a hat-type specimen in the compression test. Based on the results of finite element analysis, the employed geometry of the hat-type specimen was found to yield a load–displacement curve that is nearly independent of the friction between the specimen and the platen. The flow stress–strain curves of the alloy and tantalum were modeled using the Ludwik and Voce constitutive laws, respectively; furthermore, simulation of the compression event of the hat-type specimen was performed by assuming appropriate constitutive parameters. The constitutive parameters were varied via an optimization function built in MATLAB *until the simulated load–displacement curves reasonably fit the experimental curve. The optimized constitutive parameters obtained in this way were then used to construct friction-free flow stress–strain curves of the two materials.*
[DOI: 10.1115/1.4042138]

Keywords: constitutive relations, mechanical behavior, plastic behavior

1 Introduction

The precise calibration of the constitutive model [1–6] is a prerequisite for an accurate computer simulation of the deformation behavior of solids and structures. To calibrate a constitutive model, stress–strain curves of materials measured in a friction-free stress state (the uniform and uniaxial stress state) are needed.

Compression testing using a cylindrical specimen is probably the simplest and most handy methodology for measuring the stress–strain curve. In the compression test, however, the uniform and uniaxial stress state is manifested only when there is no friction between the specimen and the platen. When there is friction, barreling and rollover of the side wall of the specimen usually take place [7–14]. Then, the stress state of the specimen ceases to be uniaxial, becoming multi-axial and nonuniform. As a result, the stress–strain curve measured in the compression test is overestimated; the degree of overestimation increases as the height-to-diameter (H/D) ratio decreases [15–18].

The ratio of the measured flow stress (p_a) to the friction-free flow stress (σ_o) is described by an equation called the friction-compensation equation, $f(\mu, D/H)$: $p_a/\sigma_o = f(\mu, D/H)$, where μ is the Coulomb friction coefficient. An example of the friction-compensation equation developed by Schroeder and Webster (SW) [15] for the sliding contact surface is

$$\frac{p_a}{\sigma_o} = \frac{2}{\alpha^2}\left[e^{\alpha} - \alpha - 1\right] \tag{1}$$

where $\alpha = \mu D/H$. Once $f(\mu, D/H)$ is known, σ_o can be obtained from the measured flow stress under a frictional condition (p_a). Thus far, a number of other friction compensation equations have been developed [16–18]. To use these friction-compensation equations to obtain the friction-free stress–strain curve, the Coulomb friction coefficient needs to be measured separately using appropriate methodologies such as the ring compression test [19,20] and barreling compression test [21,22]; however, the reliabilities of these test methodologies have not been completely verified [20,21].

If a reliable friction coefficient is obtained, its application to the cylindrical specimen must be done carefully. According to SW [15], there are three types of contact surfaces between a cylindrical specimen and the platen: (i) the entire contact surface is sliding; (ii) there is no relative sliding on the inner zone, while the outer annular zone is sliding; and (iii) no relative sliding occurs on the entire contact surface. SW provided compensation equations for each contact surface. As for the first case when the entire contact surface is sliding, besides SW, a number of researchers

[1]Corresponding authors.

Contributed by the Applied Mechanics Division of ASME for publication in the JOURNAL OF APPLIED MECHANICS. Manuscript received September 15, 2018; final manuscript received November 22, 2018; published online January 22, 2019. Assoc. Editor: Junlan Wang.

have provided compensation equations [16–18]. To accurately compensate for the effect of friction in the measured stress–strain curve of the cylindrical specimen, information on not only the value of the friction coefficient but also the contact mechanism (the types of the contact surface) is necessary. Knowledge of the most reliable friction-compensation equation among the available equations is also necessary [15–18].

Despite the above limitations, most of the studies in the literature used cylindrical specimens to measure the compressive stress–strain curve and compensated for the influence of friction using the compensation models developed for a sliding-contact surface. For instance, Han [23], Christiansen et al. [24], and Smith and Kassner [25] used Eq. (1), i.e., the compensation equation of Schroeder and Webster [15], to compensate for the influence of friction in their quasi-static stress–strain curves. In the study of Altinbalik et al. [26], Eq. (1) was used to predict press loads in closed-die upsetting. To compensate the dynamic stress–strain curves measured using the cylindrical specimen in the split Hopkinson pressure bar test [27,28], Kamler et al. [29], Bertholf and Karnes [30], and Cha et al. [18] used the compensation models of Hill [16], Rand [17], and Cha et al. [18], respectively. Except for the study by Christiansen et al. [24], the friction coefficient was arbitrarily assumed.

Under the above circumstances, eliminating the influence of friction itself in the experimental stage of specimen deformation may be one of the desirable approaches for obtaining a friction-free stress–strain curve in the compression test. In this regard, this study considers a hat-type specimen in compression testing. To the best of our knowledge, no study has been carried out to determine a friction-free stress–strain curve using the hat-type specimen. As will be presented later in this paper, the load–displacement curve of the hat-type specimen is manifested mainly from the plastic deformation of the localized shear zone that is far from the contact surfaces; friction at the contact surfaces hardly influences local deformation in the shear zone. In this regard, this study aims to determine the friction-free stress–strain curves of an aluminum alloy and tantalum by comparing the experimental and simulation curves of the load–displacement of a hat-type specimen subjected to a compression test.

2 Methods

2.1 Numerical Simulation. The shape and axisymmetric finite element model of the hat-type specimen are presented in Fig. 1. Three-node-linear-axisymmetric triangle elements (CAX3) were used to discretize the specimen volume. The top and bottom platens were modeled using analytically rigid surfaces (not shown in Fig. 1). Two extreme values of the Coulomb friction coefficient were considered at the contact surfaces: either zero or unity. The displacement of the reference point of the top rigid surface was controlled, while the bottom rigid surface was fixed against the axial displacement. The reaction force at the reference point of the top rigid surface was monitored and was used to construct the load–displacement curve.

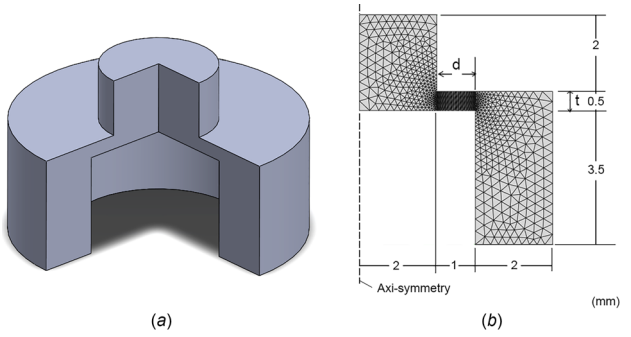

Fig. 1 (*a*) Shape of the hat-type specimen with a 90 deg cut for visualization of the inner part and (*b*) the 2D axisymmetric finite element model of the specimen

Either aluminum alloy (AA; Al 6061-T6) or tantalum (Ta) was considered as the specimen material. The elastic moduli of AA and Ta are 68.9 and 180 GPa, respectively, and their Poisson's ratios are 0.33 and 0.35, respectively. In the numerical verification of the methodology presented in this study (in Sec. 3.1), the flow stress–strain curves of AA and Ta were adapted from Refs. [31] and [32], respectively, and they were fitted using the Ludwik [1] and Voce [2] constitutive laws, respectively,

$$\sigma = a + b\varepsilon^n \tag{2}$$

$$\sigma = a + b[1 - \exp(-n\varepsilon)] \tag{3}$$

where σ is the equivalent stress in the plastic regime, ε is the equivalent plastic strain, and a, b, and n are the constitutive parameters (fitting constants). The above constitutive laws are independent of the strain rate. User subroutines (UHARD) were written to implement the respective constitutive law. A commercial finite element package (ABAQUS) was used as the solver for implicit finite element analysis. An explicit analysis was also carried out separately to determine the strain rate of the plastically deforming shear zone.

2.2 Experiment. The hat-type specimen of aluminum alloy (Al 6061-T6) was fabricated from a round bar with a diameter of 20 mm (the axial direction of the specimen coincides with the as-received bar). A rolled and annealed tantalum plate with a thickness of 10 mm was machined to the hat-type specimen (the axial direction of the specimen is the thickness direction in the as-received plate).

Compression testing of the hat-type specimens was carried out using a universal mechanical tester with stainless steel platens and a 3 ton-force load cell (Instron 3361). Tungsten carbide (with 6 wt % Co) disks with a diameter of 25.4 mm and thickness of 5 mm were inserted between the top/bottom platens and specimen. An aliquot of lubricant was applied to the contact surfaces between the specimen and the tungsten carbide disks. The compression test was carried out at the cross-head speed of 0.01 mm/min.

2.3 Optimization of the Constitutive Parameters. The flow chart for the optimization process used to determine the friction-free stress–strain curve is illustrated in Fig. 2. The load–displacement curve of the hat-type specimen of either

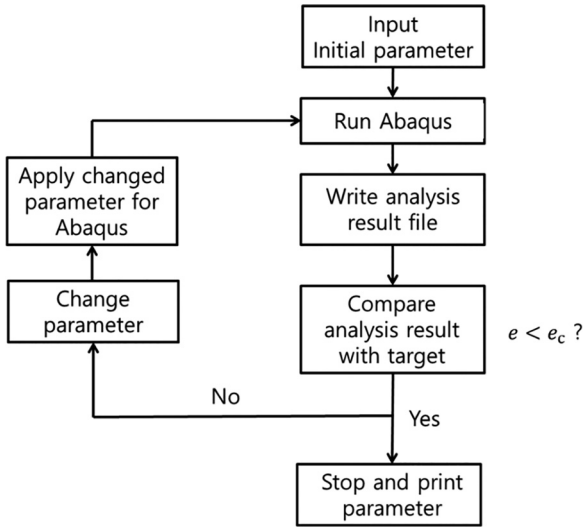

Fig. 2 Schematic illustration of the optimization process for the constitutive parameters. e_c is the predefined error level.

aluminum alloy (AA) or tantalum (Ta) was used as the target function. The stress–strain curves of the specimen materials to be determined were modeled using either the Ludwik or the Voce constitutive law.

A governing program written in Python script selects the constitutive parameters using an optimization algorithm (the function "fminsearch" built in MATLAB), while initially guessed parameters are set by the user of the program. The program then runs the finite element (FE) package (ABAQUS) using the selected parameters. After the simulation is finished, the program compares the simulated load–displacement curve with the target function to calculate the value of the error (e), which is defined by the following equation:

$$e = \frac{\sum_{i=1}^{N} \left(F^i_{\text{target}} - F^i_{\text{simulated}} \right)^2}{\sum_{i=1}^{N} \left(F^i_{\text{target}} \right)^2} \tag{4}$$

where F^i_{target} and $F^i_{\text{simulated}}$ are the target and simulated forces, respectively, i is the index of data points, and N is the number of data points used in the optimization process.

If the value of the error is larger than the predefined level (e_c), the governing program reselects the constitutive parameters based on the optimization algorithm and reruns the FE package. If the error value is less than the predefined value, it outputs the constitutive parameters that were used in the final simulation. The stress–strain curve of the specimen material is constructed (uncovered) using the optimized constitutive parameters that were used in the final simulation.

3 Results and Discussion

3.1 Numerical Verification of the Methodology. To numerically verify the presented methodology, the flow stress–strain curves of AA and Ta available in the literature [31,32] were used as the input properties of the specimen materials. The deformed shapes of the hat-type specimens (for AA and Ta) obtained via numerical simulation (implicit finite element analysis) of the compression test are presented in Fig. 3 with contours of the equivalent plastic strain ($\mu = 0$). As can be observed in Fig. 3, deformation is concentrated in the shear zone, which is far from the contact surfaces. When the friction coefficient was set as unity, no appreciable differences were observed in the deformed shape and contour (not shown).

The load–displacement curves obtained in the numerical simulation are presented in Fig. 4(*a*) for AA and Ta. Although the friction coefficient was changed from zero to unity (extreme case), the load–displacement curves are almost the same regardless of the value of the friction coefficient at the contact surfaces. This is

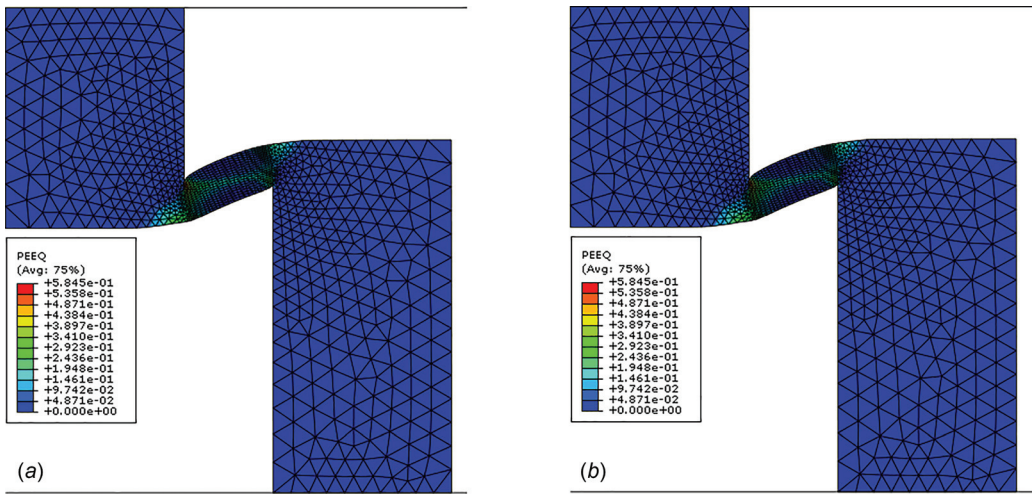

Fig. 3 Simulated deformed shapes and contours of the equivalent plastic strain of the hat-type specimens of (*a*) aluminum alloy (AA) and (*b*) tantalum (Ta) at the displacement value of 0.5 mm (the value of the friction coefficient was set as zero)

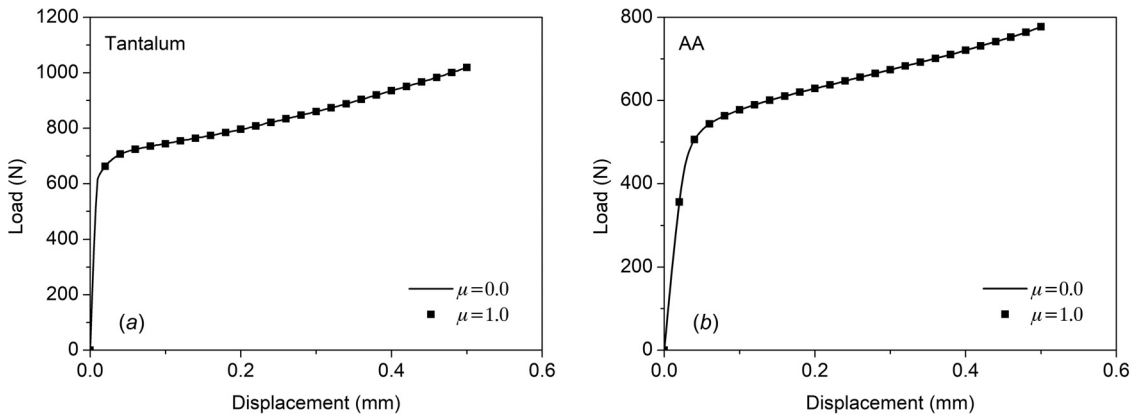

Fig. 4 Load–displacement curves of (*a*) aluminum alloy (AA) and (*b*) tantalum (Ta) obtained via numerical simulation for the cases when $\mu = 0$ and $\mu = 1$

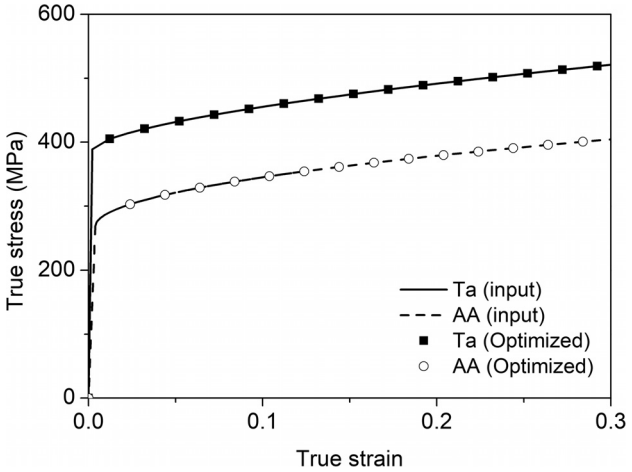

Fig. 5 Stress–strain curves (closed squares and open circles) obtained via the optimization process using the load–displacement curves in Fig. 4. The solid and dashed curves are the input properties of the respective material used to obtain the load–displacement curve via the simulation (target function; Fig. 4).

because the deformation of the shear zone is mainly responsible for the manifestation of the load–displacement curve, while friction at the contact surfaces does not influence the shear deformation that occurs in local areas far from the contact surfaces. If the stress–strain curve is extracted from such a friction-independent load–displacement curve, the obtained stress–strain curve should be a friction-free property of the material.

To determine the flow stress–strain curves that resulted in the respective load–displacement curves in Fig. 4, the flow stress–strain curves of AA and Ta were modeled using the Ludwik and Voce constitutive laws, respectively. Then, a numerical simulation of the compression test of the hat-type specimen was carried out by assuming appropriate constitutive parameters. The constitutive parameters were optimized via the process described in Fig. 2. The stress–strain curves constructed using the determined parameters are presented in Fig. 5 as closed squares. Figure 5 shows the solid and dashed curves that indicate the input properties of the respective material used to obtain the load–displacement curves of Fig. 4 via the simulation (the target function).

As can be observed in Fig. 5, the stress–strain curves determined via the parameter optimization process (data points) are consistent with the input properties used for obtaining the target function via the simulation. This finding verifies that the determined stress–strain curves of AA and Ta from the load–displacement curves of the hat-type specimen via the parameter optimization process are reliable. The stress–strain curve obtained in this way is a friction-free property of the specimen material.

Table 1 Determined constitutive parameters for aluminum alloy and tantalum.

Material	Constitutive law	a (MPa)	b (MPa)	n
Aluminum alloy (AA)	Ludwik (Eq. (2))	268.2218	252.9981	0.5087
Tantalum (Ta)	Voce (Eq. (3))	407.6501	342.0435	1.3441

3.2 Experimental Determination of the Friction-Free Stress–Strain Curve. The experimentally obtained load–displacement curves of AA and Ta are presented in Fig. 6(*a*) as solid curves. They were used as the target functions in the parameter optimization process. The flow stress–strain curves of AA and Ta to be determined were modeled using the Ludwik and Voce constitutive laws, respectively. The constitutive parameters were extracted when the simulated load–displacement curves were consistent with the target functions shown in Fig. 6(*a*).

The constitutive parameters determined in this way are presented in Table 1. These parameters were used to construct the stress–strain curves of the respective materials, and the results are presented in Fig. 6(*b*) as solid and dashed curves. Included in Fig. 6(*b*) are data points (closed squares) that indicate the stress–strain curve of Al6061-T6 adapted from Ref. [31]. This alloy is produced through a well-regulated process, and thus, the mechanical properties of the AA alloy (Al6061-T6) used in this study are believed to be the same as those of the alloy used in Ref. [31]. The proximity of the data points (Ref. [31]) and red solid curve (determined in this study) indicates again the reliability of the stress–strain curve determined in this study.

Figure 6(*b*) also presents the stress–strain curve of tantalum determined in this study (black solid curve). Based on the numerical verification for tantalum in Sec. 3.1 and the proximity of the closed squares and solid curve in Fig. 6(*b*), the determined stress–strain curve of tantalum in Fig. 6(*b*) is believed to be reliable: it is the friction-free stress–strain curve of tantalum used in this study. There is no comparison standard for the solid curve in Fig. 6(*b*) because, like those of other metallic materials, the mechanical properties of tantalum are dependent on the manufacturing process (e.g., the degree of rolling, heat treatment time, and heat treatment temperature), which yields different microstructures.

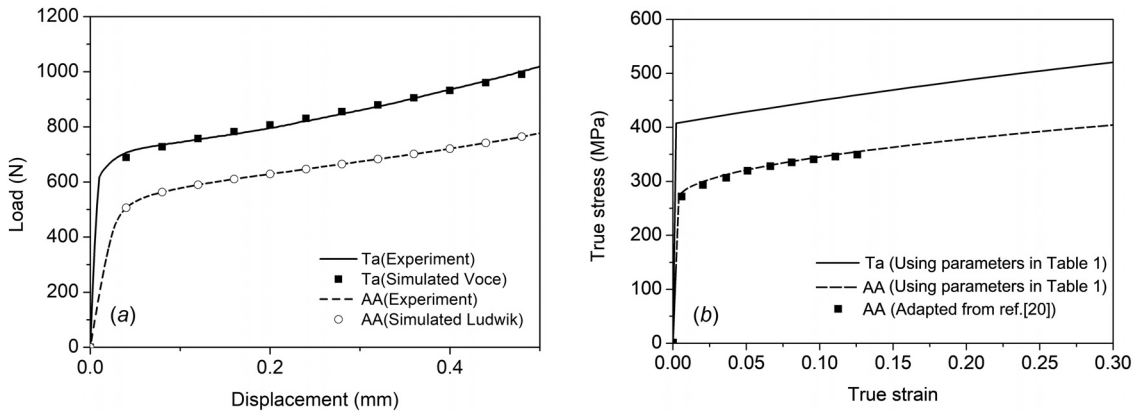

Fig. 6 (*a*) Experimentally obtained load–displacement curves of the aluminum alloy and tantalum (solid curves). Simulated load–displacement curves when the parameter optimization was completed (data points). (*b*) Determined stress–strain curves (solid curves) in this study using the optimized constitutive parameters presented in Table 1.

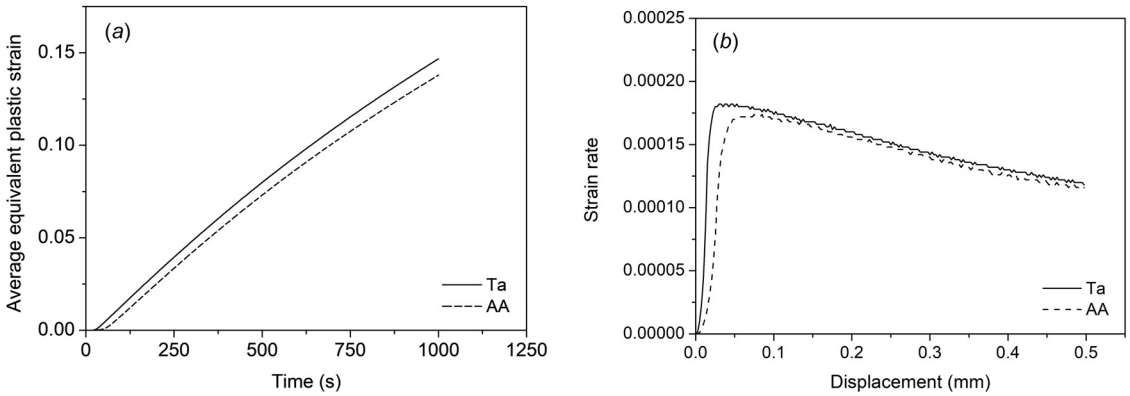

Fig. 7 (*a*) Average equivalent plastic strain versus time obtained via explicit finite element analysis using the constitutive parameters in Table 1. (*b*) Time derivative of the curve in (*a*).

3.3 Shape Design of the Hat-Type Specimen. For the geometry considered in this study (Fig. 1), the load–displacement curve was independent of the friction coefficient between the hat-type specimen and the top/bottom platen (Fig. 4). Such a friction-independent load–displacement curve can be obtained using other geometries of the hat-type specimen as well. Based on a separate simulation (not shown), the hat-type geometry with a t value of 1 mm and a d value of 2 mm also yielded the friction-independent load–displacement curve (the definition of t and d is shown in Fig. 1). If the value of d is insufficient at a given value of t, the load–displacement curve tends to show friction dependency. Using this information, researchers may suitably design their own geometries of the hat-type specimen to achieve a friction-independent load–displacement curve and verify the geometries via FE analysis (Fig. 4).

3.4 Strain-Rate Dependency in the Quasi-Static Regime. In the quasi-static strain-rate regime, the strain-rate dependency of the flow stress of a metallic material is generally described by the following rate-dependent constitutive laws [3,4]:

$$\sigma = [a + b\varepsilon^n]\left[1 + c\ln\frac{\dot{\varepsilon}}{\dot{\varepsilon}_o}\right] \tag{5}$$

$$\sigma = \left[a + b\left\{1 - \exp(-n\varepsilon)\right\}\right]\left[1 + c\ln\frac{\dot{\varepsilon}}{\dot{\varepsilon}_o}\right] \tag{6}$$

where c is the fitting parameter (called the rate constant), $\dot{\varepsilon}$ is the strain rate, and $\dot{\varepsilon}_o$ is the reference strain rate at which the constitutive model is calibrated (a setting constant in the calibration process of the constants a, b, n, and c). The constitutive parameters can be determined via nonlinear curve fitting of two or more stress–strain curves measured at two or more different strain rates (e.g., 10^{-5} and 10^{-2} s^{-1}). In Eqs. (5) and (6), the first bracket in each equation describes the flow stress–strain curve at the reference strain rate. According to Eqs. (5) and (6), the flow stress increases linearly with an increase in the value of $\ln\dot{\varepsilon}$. The value of c is fairly small for most metallic materials: the rate dependency of the flow stress–strain curve is negligible in the quasi-static strain rate regime. For instance, the values of c are 0.025 for OFHC [3] and 0.011 for the Al 6082 alloy [33]. When we calculated the value of c using the data for Al 6061-T6 [34], it was 0.0011.

Nevertheless, in case the strain rate of the obtained stress–strain curve is needed for the calibration of the rate parameter (c) in the quasi-static strain-rate regime, one may simulate the compression event of the hat-type specimen via *explicit* finite element analysis. In this study, explicit finite element analysis was carried out using Eqs. (2) and (3) and the parameters in Table 1 which were determined via an implicit analysis. For a more rigorous determination of the strain rate, we need to carry out the parameter optimization process itself via explicit finite element analysis using the constitutive laws of Eqs. (5) and (6), which imposes an overly extensive computational burden than the optimization process based on an implicit analysis. It is desirable to carry out the optimization process using an implicit analysis like in this study and carry out an explicit analysis later (separately) using the parameters determined through the implicit analysis.

In this study, after carrying out an explicit analysis using the parameters in Table 1, the values of the equivalent plastic strain in the shear zone defined by $d \times t$ in Fig. 1(*b*) were extracted and averaged. The averaged value of the equivalent plastic strain as a function of time is presented in Fig. 7(*a*). In Fig. 7(*a*), the (average equivalent) *plastic* strain of AA starts to increase later than that of Ta because AA has a lower elastic modulus than Ta.

The slopes of the curves in Fig. 7(*a*) are presented in Fig. 7(*b*). In Fig. 7(*b*), it may be appropriate to determine the strain rate after its value reaches a maximum, i.e., after the equivalent plastic strain starts to increase in Fig. 7(*a*). For the case of AA, the strain rate gradually decreases from approximately 1.7×10^{-4} to 1.2×10^{-4} s^{-1}; one may select the average value of 1.45×10^{-4} s^{-1} as the strain rate of the obtained stress–strain curves (Fig. 6(*b*)). For the case of Ta, the average value of the strain rate is approximately 1.5×10^{-4} s^{-1}. If the cross-head speed increases, the strain rate in the shear zone increases correspondingly.

4 Conclusion

The numerical simulation of the compression test for the hat-type specimen employed in this study indicates that the load–displacement curve is independent of friction between the top/bottom platens and the specimen. This finding means that if a stress–strain curve is extracted from the measured load–displacement curve, the obtained stress–strain curve is a friction-free property of the material.

This study numerically verified the following process for obtaining a friction-free stress–strain curve of a specimen material from the load–displacement curve of the hat-type specimen. The flow stress–strain curve of the specimen material to be determined is modeled using either the Ludwik or the Voce constitutive law. Then, a numerical simulation for the experimental process is carried out by assuming appropriate constitutive parameters of the specimen material. The simulation is repeated until the simulated load–displacement curve is reasonably coincident to the experimentally obtained load–displacement curve (the target function). The constitutive parameters are extracted when the simulated load–displacement curve is consistent with the target function. The optimized constitutive parameters in this way are used to construct the friction-free stress–strain curve.

Based on the above process, friction-free stress–strain curves of aluminum alloy (Al 6061-T6) and tantalum were experimentally determined. For the case of the aluminum alloy, the

experimentally determined flow stress–strain curve in this study was consistent with the one reported in the literature, verifying the reliability of the proposed process using the hat-type specimen.

As for the design guideline for the hat-type specimen, if the value of d is insufficient at a given value of t (d and t are defined in Fig. 1), the load–displacement curve tends to show friction dependency. With this knowledge, researchers may suitably design their own geometries of the hat-type specimen to achieve a friction-independent load–displacement curve and verify the geometries via FE analysis.

In case the strain rate of the determined stress–strain curve is needed, it is desirable to carry out the optimization process using an implicit analysis, such as in this study, and carry out the explicit analysis later (separately) using the parameters determined in the implicit analysis. After the explicit analysis, the average value of the equivalent plastic strain in the shear zone can be extracted as a function of time, and the slope of the curve in the plastic regime can be averaged to obtain the strain rate.

References

[1] Ludwik, P., 1909, *Elemente Der Technologisehen Mechanik (Elements of Technological Mechanics)*, Springer, Berlin, p. 32.

[2] Voce, E., 1948, "The Relationship Between Stress and Strain for Homogeneous Deformation," J. Inst. Met., **74**, pp. 537–562.

[3] Johnson, G. R., and Cook, W. H., 1983, "A Constitutive Model and Data for Metals Subjected to Large Strains, High Strain Rates and High Temperatures," Seventh International Symposium on Ballistics. Hague: Organizing Committee of the seventh ISB, The Hague, The Netherlands, Apr. 19–21, pp. 541–547.

[4] Shin, H., and Kim, J.-B., 2010, "A Phenomenological Constitutive Equation to Describe Various Flow Stress Behaviors of Materials in Wide Strain Rate and Temperature Regimes," ASME J. Eng. Mater. Technol., **132**(2), p. 021009.

[5] Gross, A. J., and Ravi-Chandar, K., 2015, "On the Extraction of Elastic–Plastic Constitutive Properties From Three-Dimensional Deformation Measurements," ASME J. Appl. Mech., **82**(7), p. 071013.

[6] Yafu, F., Wang, Q.-D., Ning, J.-S., Chen, J., and Wei, J., 2010, "Experimental Measure of Parameters: The Johnson–Cook Material Model of Extruded Mg–Gd–Y Series Alloy," ASME J. Appl. Mech., **77**(5), p. 051902.

[7] Felling, A. J., and Doman, D. A., 2018, "A New Video Extensometer System for Testing Materials Undergoing Severe Plastic Deformation," ASME J. Eng. Mater. Technol., **140**(3), p. 031005.

[8] Krishna, C. H., Davidson, M. J., Nagaraju, C., and Kumar, P. R., 2015, "Effect of Lubrication in Cold Upsetting Using Experimental and Finite Element Modeling," J. Test. Eval., **43**(1), pp. 53–61.

[9] Misirili, C., 2014, "On Materials Flow Using Different Lubricants in Upsetting Process," Ind. Lub. Tribol., **66**(5), pp. 623–631.

[10] Banerjee, J. K., 1985, "Barreling of Solid Cylinders Under Axial Compression," ASME J. Eng. Mater. Technol., **107**(2), pp. 138–144.

[11] Banerjee, J. K., and Cárdenas, G., 1985, "Numerical Analysis on the Barreling of Solid Cylinders Under Axisymmetric Compression," ASME J. Eng. Mater. Technol., **107**(2), pp. 145–147.

[12] Lee, C. H., and Altan, T., 1972, "Influence of Flow Stress and Friction Upon Metal Flow in Upset Forging of Rings and Cylinders," ASME J. Eng. Ind., **94**(3), pp. 775–782.

[13] Kim, S., Kim, M., Shin, H., and Rhee, K. Y., 2018, "Measurement of a Nearly Friction-Free Stress–Strain Curve of Silicone Rubber Up to a Large Strain in Compression Testing," Exp. Mech., **58**(9), pp. 1479–1484.

[14] Tan, X., 2011, "Evaluation of Friction in Upsetting," Prod. Eng., **5**(2), pp. 141–149.

[15] Schroeder, W., and Webster, D. A., 1949, "Press-Forging Thin Sections: Effect of Friction, Area, and Thickness on Pressure Required," ASME J. Appl. Mech., **16**, pp. 289–294.

[16] Hill, R., 1950, *The Mathematical Theory of Plasticity*, Oxford University Press, London, pp. 262–281.

[17] Rand, J. L., 1967, "An Analysis of the Split Hopkinson Pressure Bar," Technical Report, U.S. Naval Ordnance Laboratory, Silver Spring, MD, Report No. NOLTR 67-156.

[18] Cha, S.-H., Shin, H., and Kim, J.-B., 2010, "Numerical Investigation of Frictional Effects and Compensation of Frictional Effects in Split Hopkinson Pressure Bar (SHPB) Test (in Korean)," Trans. Korean Soc. Mech. Eng., A., **34**(5), pp. 511–518.

[19] Hu, C., Ou, H., and Zhao, Z., 2015, "An Alternative Evaluation Method for Friction Condition in Cold Forging by Ring With Boss Compression Test," J. Mater. Process. Technol., **224**, pp. 18–25.

[20] Sofuoglu, H., Gedikli, H., and Rasty, J., 2001, "Determination of Friction Coefficient by Employing the Ring Compression Test," ASME J. Eng. Mater. Technol., **123**(3), pp. 338–348.

[21] Solhjoo, S., 2010, "A Note on 'Barrel Compression Test': A Method for Evaluation of Friction," Comput. Mater. Sci., **49**(2), pp. 435–438.

[22] Yao, Z., Mei, D., Shen, H., and Chen, Z., 2013, "A Friction Evaluation Method Based on Barrel Compression Test," Tribol. Lett., **51**(3), pp. 525–535.

[23] Han, H., 2002, "The Validity of Mechanical Models Evaluated by Two-Specimen Method Under the Known Coefficient of Friction and Flow Stress," J. Mater. Process. Technol., **122**(2–3), pp. 386–396.

[24] Christiansen, P., Martins, P. A. F., and Bay, N., 2016, "Friction Compensation in the Upsetting of Cylindrical Test Specimens," Exp. Mech., **56**(7), pp. 1271–1279.

[25] Smith, K. K., and Kassner, M. E., 2016, "Through-Thickness Compression Testing of Commercially Pure (Grade II) Titanium Thin Sheet to Large Strains," J. Metall., **2016**, p. 6178790.

[26] Altinbalik, T., Akata, H., and Can, Y., 2007, "An Approach for Calculation of Press Loads in Closed-Die Upsetting of Gear Blanks of Gear Pumps," Mater. Des., **28**(2), pp. 730–734.

[27] Al-Mousawi, M. M., Reid, S. R., and Deans, W. F., 1997, "The Use of the Split Hopkinson Pressure Bar Techniques in High Strain Rate Materials Testing," Proc. Inst. Mech. Eng., Part C, **211**(4), pp. 273–292.

[28] Shin, H., and Kim, J.-B., 2019, "Evolution of Specimen Strain Rate in Split Hopkinson Bar Test," Proc. Inst. Mech. Eng., Part C: J. Mech. Eng. Sci. https://doi.org/10.1177/0954406218813386

[29] Kamler, F., Niessen, P., and Pick, R. J., 1995, "Measurement of the Behaviour of High Purity Copper at Very High Rates of Straining," Can. J. Phys., **73**(5–6), pp. 295–303.

[30] Bertholf, L. D., and Karnes, C. H., 1975, "Two-Dimensional Analysis of the Split Hopkinson Pressure Bar System," J. Mech. Phys. Solids., **23**(1), pp. 1–19.

[31] Ambriz, R. R., Mesmacque, G., Ruiz, A., Amrouche, A., and Lopez, V. H., 2010, "Effect of Welding Profile Generated by the Modified Indirect Electric Arc Technique on the Fatigue Behavior of 6061-T6 Aluminum Alloy," Mater. Sci. Eng., A., **527**(7–8), pp. 2057–2064.

[32] Chen, S. R., and Gray Ill, G. T., 1996, "Constitutive Behavior of Tantalum and Tantalum-Tungsten Alloys," Metall. Mater. Trans., A, **27**(10), pp. 2994–3006.

[33] Lemanski, S. L., Petrinic, N., and Nurick, G. N., 2013, "Experimental Characterisation of Aluminium 6082 at Varying Temperature and Strain Rate," Strain, **49**(2), pp. 147–157.

[34] Hoge, K. G., 1966, "Influence of Strain Rate on Mechanical Properties of 6061-T6 Aluminum Under Uniaxial and Biaxial States of Stress," Exp. Mech., **6**(4), pp. 204–211.